forests

MDPI

Article

Characteristics, Sources, and Mechanisms of Soil Respiration under Simulated Rainfall in a Native Karst Forest in Southwestern China

Wenqiang Lv [1], Xiuming Liu [2,*] and Hu Ding [3,*]

[1] School of Geography and Resources, Guizhou Education University, Guiyang 550018, China; lvwenqiang@gznc.edu.cn
[2] State Key Laboratory of Environmental Geochemistry, Institute of Geochemistry, Chinese Academy of Sciences, Guiyang 550081, China
[3] School of Earth System Science, Tianjin University, Tianjin 300072, China
* Correspondence: liuxiuming@vip.skleg.cn (X.L.); dinghu@tju.edu.cn (H.D.)

Abstract: Rainfall significantly affects soil respiration rates by altering microbial activity and organic matter decomposition. In karst regions, it also impacts carbonate dissolution and precipitation, further influencing soil CO_2 flux. Investigating the mechanism of rainfall's impact on soil respiration is essential for accurately evaluating and predicting changes in terrestrial ecosystems. However, our understanding of the interaction between rainfall and soil respiration in the extensive karst ecosystems of southwestern China remains limited. This study conducted field-based simulated rainfall experiments to examine variations in soil respiration rates and elucidate the associated control mechanisms through stable carbon isotope composition analysis. Simulated rainfall significantly increased the CO_2 release via soil respiration. We observed significant differences in the $\delta^{13}C$ value of soil-respired CO_2 before and after simulated rainfall. Following the rain, the $\delta^{13}C$ of soil-respired CO_2 was enriched compared to that before the rain. Through isotope data analysis, we found that the increased soil CO_2 emissions were primarily driven by heterotrophic respiration, likely stimulated via changes in soil moisture, affecting microbial growth conditions. Furthermore, the variation in soil moisture affected carbonate dissolution and precipitation, potentially increasing the soil CO_2 release after rainfall. In conclusion, these findings expand our understanding of rainfall's effects on soil respiration in the native karst forests of southwestern China, contributing to the prediction of carbon cycling processes in such ecosystems. The data from this study have significant implications for addressing the release of greenhouse gases in efforts to combat climate change.

Keywords: soil respiration; karst forest; simulated rainfall; CO_2 emissions; stable carbon isotope

check for updates

Citation: Lv, W.; Liu, X.; Ding, H. Characteristics, Sources, and Mechanisms of Soil Respiration under Simulated Rainfall in a Native Karst Forest in Southwestern China. *Forests* **2024**, *15*, 945. https://doi.org/10.3390/f15060945

Academic Editor: Adele Muscolo

Received: 4 May 2024
Revised: 26 May 2024
Accepted: 28 May 2024
Published: 30 May 2024

Copyright: © 2024 by the authors. Licensee MDPI, Basel, Switzerland. This article is an open access article distributed under the terms and conditions of the Creative Commons Attribution (CC BY) license (https://creativecommons.org/licenses/by/4.0/).

1. Introduction

Climate change is the most formidable global challenge confronting human society in the 21st century. Thus, mitigating the atmospheric greenhouse effect is a pressing global environmental issue. The soil release of CO_2, or soil respiration (SR), is recognized as a major carbon flux in the global carbon cycle. As the largest carbon pool in terrestrial ecosystems [1,2], soil carbon reservoirs are the primary source of soil CO_2 emissions [3]. Even minor shifts in soil respiration can have a major impact on atmospheric CO_2 concentrations [4] and global carbon cycling. Thus, understanding soil respiration processes will play a critical role in climate change mitigation.

Soil respiration is highly sensitive to variations in precipitation patterns [5,6]. Changes in precipitation quantity, frequency, and seasonal distribution exert a powerful influence on soil respiration dynamics [7,8]. However, numerous factors affect the response of soil respiration to rainfall, including precipitation volume, initial soil moisture conditions [9], climatic regions [10,11], ecosystem types [12], and rainfall frequency [13]. These variables

contribute to significant uncertainties that hamper the ability to forecast rainfall effects on soil respiration across various ecosystems [12].

Soil respiration has two main sources: autotrophic soil respiration (SR_a) and heterotrophic soil respiration (SR_h) [14]. The latter describes the breakdown of soil organic carbon (SOC) via soil organisms [15–17], whereas the former is closely related to activity from plant roots and associated biota [16,18]. The responses of SR_h and SR_a to precipitation patterns vary across ecosystem types and climatic regions [19–27]. Understanding how soil components involved in respiration react to precipitation dynamics is essential in assessing climate–carbon cycle feedback [28].

Stable isotope fractionation provides valuable insight into ecological responses under environmental fluctuation across temporal and spatial scales. It is extensively used to quantify eco-processes associated with carbon cycling [29–32]. For instance, SR_a exhibits minimal carbon fractionation and, thus, produces CO_2 with $\delta^{13}C$ values that have similar characteristics as its source of plant root tissues [33], whereas SR_h mirrors the $\delta^{13}C$ values of soil organic matter [30,34]. Measuring naturally abundant stable carbon isotopes holds substantial promise for discerning soil respiration components [32,35–39]. Furthermore, given the diverse response mechanisms of soil respiration to precipitation, rainfall events should lead to quantifiable $\delta^{13}C$ variation that has the potential to clarify effects on various soil components.

Carbonate rocks exhibit a global distribution, spanning an estimated area of 22 million square kilometers, which accounts for approximately 15% of the total land area [40]. Carbonate rocks are the primary carbon reservoirs in the Earth's surface system, with an estimated storage of around (50–120) $\times$ 10^6 PgC [41]. The karst carbon cycle plays a significant role in the global carbon cycle and demonstrates a high level of sensitivity to environmental variations. It is intricately connected to the carbon cycle of terrestrial ecosystems, the soil carbon cycle, and changes in land use. It represents a crucial and substantial element of the global carbon cycle. Karst ecosystems are widely distributed throughout the carbonate rocks of Southwest China. The carbon cycle in these ecosystems, influenced by karst rocks, is characterized by the complex interplay between the surface and subsurface double-layer structure, the integration of organic and inorganic carbon cycles, and the interdependence of biotic and abiotic processes. The intricate characteristics of karst ecosystems make them exceptionally unique and complex compared to other terrestrial ecosystems [42]. Our knowledge regarding how soil respiration responds to rainfall in these specialized regions remains limited. Furthermore, important questions to address include whether autotrophic and heterotrophic respiration differ in their responses, as well as whether inorganic carbon sources contribute to soil CO_2 emissions.

To address these topics, this study aimed to perform simulated rainfall experiments in a native karst forest of southwestern China. We analyzed soil respiration rates and stable carbon isotopes to clarify the response of soil CO_2 emissions to precipitation. Our findings provide broader insights into the soil carbon cycling of karst ecosystems and a scientific basis for assessing how rainfall variation under climate change influences the carbon balance in an understudied environment.

2. Materials and Methods

2.1. Study Area

Data were collected from the Maolan observation site at the Puding Karst Ecosystem Research Station of the Chinese Academy of Sciences (Figures 1 and 2), situated in a sloping transition zone from the southern Guizhou Plateau to the hilly plains of Guangxi (107°37′–108°18′ E and 25°07′–25°39′ N). The forest area comprises limestone and dolomite rocks, with a bare rock exposure rate of 70%–80%. The average annual temperature is 15.3 °C, and the climate is that of a subtropical monsoon. Rainfall from April to September can reach 1420 mm, constituting 81% of the total annual precipitation, with the period from June to August alone contributing 96%–97%. This region contains the only remaining primitive and relatively stable karst forest ecosystem within its latitudinal zone, encom-

passing the largest area of native forest in karst regions. The predominant vegetation is arboreal forests, reaching heights of 10–20 m with over 80% canopy coverage. Key species include *Platycarya longipes*, *Pittosporum brevicalyx*, *Machilus microcarpa*, *Pteroceltistatarinowii*, *Pittosporun glabratum*, and *Castanopsis fargesii*; all of them contribute to a shalloweaf litter layer. The soil type in the experimental area was classified as limestone with a soil layer depth of approximately 30–40 cm. For detailed soil properties, see Table 1.

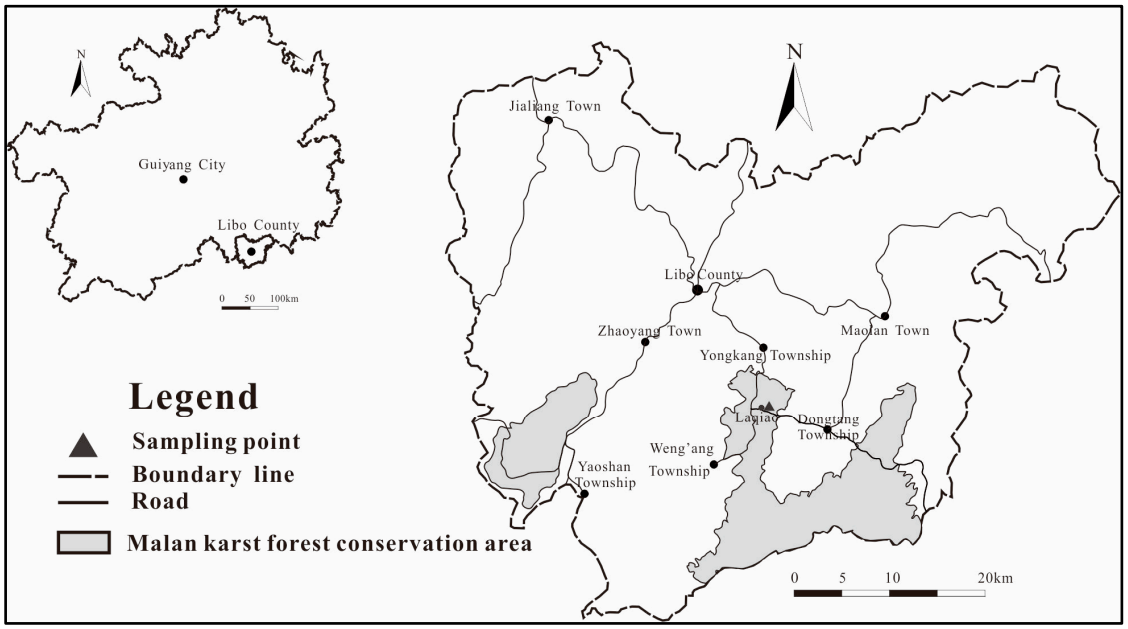


Figure 1. Location of sampling points.

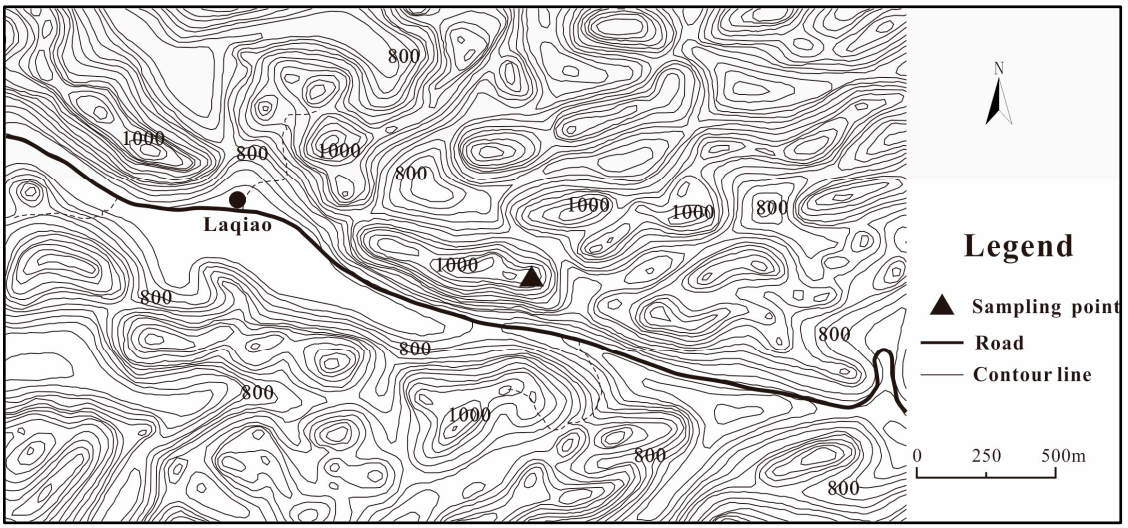


Figure 2. Topographic map of sampling points.

Table 1. Physical and chemical soil properties at sampling site.

	pH	SOC (%)	N (%)	Clay (%)	Silt (%)	Sand (%)
0–10 cm	7.94	7.35	0.60	17.3	53.7	29.0
10–20 cm	7.53	7.56	0.76	11.6	67.6	20.7

2.2. Simulated Rainfall Treatment

The research area is characterized by a major expansion of exposed bedrock and an undulating topography that has led to a highly intricate landscape with varied habitat types. A fixed experimental plot measuring 1 × 1 m was established on the soil surface; this size was selected because it covered the largest area within a small habitat (extending over 60% of the total soil surface area and reaching approximately 40 cm deep into the soil layer). To simulate rainfall, a watering can was used at the experimental site, comprising a watering unit equipped with evenly distributed small holes. The spraying speed was carefully regulated to prevent surface runoff.

The analysis of rainfall records across 40 years revealed that 87.6% of the precipitation in the sampling area occurred between April and October. In contrast, the precipitation levels in December, January, and February were minimal (5.96% of the annual rainfall). Simultaneously, in association with the prevailing weather conditions, characterized by a lack of rain or minimal precipitation in the days preceding the simulated rainfall event, three rainfall events were simulated on 14 November 2008, 30 April 2009, and 6 June 2009 (see Table 2 for rainfall characteristics), using 8, 25, and 25 mm of water, respectively.

Table 2. Simulated rainfall day, duration, and amount.

Rainfall Day	Duration	Amount of Rain
14 November 2008	20 min	8 mm
30 April 2009	20 min	25 mm
6 June 2009	20 min	25 mm

2.3. Sample Collection and Analysis

To address the influence of soil heterogeneity on the research outcomes, an in situ observation method was utilized in this study. Gas samples from soil respiration were collected using a static chamber (20 cm in diameter and 20 cm in height) at 1, 2, 4, 6, 8, 12, 16, 20, and 24 h after the rainfall simulation. Samples were also obtained at the same time points pre-rainfall for comparative analysis. The specific operation was as follows: at 0, 10, 20, and 30 min after the cover box was sealed each time, the static box was sealed with a cover to create a sampling gas chamber. The center of the ceiling cover was equipped with a sampling device that included a glass tube, a rubber hose, a three-way tube, a gas sampling bag, and a syringe. The gas in the gas chamber was transferred to the sampling bag using a three-way tube, collecting approximately 500 mL of gas. Simultaneously, soil samples from the 0–10 cm depth were collected, placed in pre-dried and weighed aluminum boxes, and transported to the laboratory to determine the soil moisture content. The soil temperature (5 cm) and ambient temperature (see Table 3) were also measured.

Table 3. Ambient temperature in static chamber before and after simulated rainfall (°C).

Time (h)	Before Simulated Rainfall			After Simulated Rainfall		
	a	b	c	a	b	c
1	19.2	14.8	23.0	19.7	18.4	25.6
2	20.4	15.6	24.2	20.9	18.2	29.2
4	19.0	16.0	26.7	18.3	18.3	29.8
6	17.9	16.0	29.0	17.4	18.3	29.6
8	14.1	15.8	29.2	14.8	18.5	29.2
12	10.3	16.2	25.2	10.6	18.6	26.3
16	10.2	16.6	23.5	12.1	18.8	25.1
20	9.2	16.6	23.8	12.5	18.6	23.8
24	16.4	17.9	22.3	18.5	19.0	22.9

a: 8 mm simulated rainfall. b: 25 mm simulated rainfall in April. c: 25 mm simulated rainfall in June.

A small portion of the sampled gas was analyzed using an HP6890 gas chromatograph (HP Corp., Palo Alto, CA, USA). The parameters for quantification in gas chromatography are presented in Table 4. The remainder was purified using a self-constructed vacuum gas-purification system equipped with a fine needle, followed by CO_2 purification in alcohol–liquid nitrogen and liquid nitrogen traps. Finally, purified gas was collected into crushable glass ampules. The stable carbon isotope composition was analyzed in a MAT-252 mass spectrometer (Thermo Finnigan Corp., San Jose, CA, USA), with the international standard Pee Dee Belemnite (PDB) as the reference. The measurement error was less than 0.05‰, and carbon isotope values ($\delta^{13}C$) were reported in the internationally accepted format:

$$\delta^{13}C = \left[R_{sample} - R_{standard}\right] / R_{standard} \times 1000‰ \quad (1)$$

where $\delta^{13}C$ represents sample carbon isotope composition, and R_{sample} and $R_{standard}$ refer to $^{13}C/^{12}C$ values in the sample and reference material, respectively, with an analysis error <0.05‰.

Table 4. Determination of CO_2 concentration via gas chromatography.

	CO_2
Chromatographic column	Porapak Q (80/100 mesh; diameter: 3.15 mm; length: 3 m)
Carrier gas	High-purity N_2
Carrier gas flow rate ($mL \cdot min^{-1}$)	20
Column box temperature (°C)	50
Converter/temperature (°C)	Nickel converter/375
Flame ionization detector/temperature (°C)	FID/250
Air/H_2 flow rate ($mL \cdot min^{-1}$)	350/30

The formula for calculating the flux of the CO_2 release (F) is as follows:

$$F = \frac{M}{V_0} \times \frac{P}{P_0} \times \frac{T_0}{T} \times H \times \frac{dc}{dt} \quad (2)$$

where F represents the flux of CO_2 emissions ($mg \cdot m^{-2} \cdot h^{-1}$), M denotes the molar mass of CO_2 under standard conditions (44 $g \cdot mol^{-1}$), H stands for the height of the sampling chamber (m), P indicates the atmospheric pressure at the sampling site (kPa), P_0, V_0, and T_0 correspond to the standard atmospheric pressure, volume, and absolute air temperature (101.325 kPa, 22.41 $L \cdot mol^{-1}$, and 273.15 K, respectively), T is the temperature at the sampling site during sampling (K), and dc/dt represents the slope of the CO_2 concentration change over time.

Determination of soil water content. The soil water content was determined using an oven-drying method. Fresh soil (~10 g) was weighed, placed in an aluminum container of known weight (accurate to 0.01 g), and then dried in a 105 ± 2 °C oven until reaching a constant weight (approximately 12 h). The container was then cooled in a desiccator for 20 min, removed from the desiccator, covered, and reweighed with a precision of 0.01 g. Three replicates were set up for each time point in the soil moisture content test.

Soil temperature measurement. The soil temperature at a 5 cm depth was measured directly using a needle-type soil thermometer (Spectrum Technologies Inc., Augusta, GA, USA). The soil temperature was measured simultaneously with the collection of soil respiration gas.

2.4. Measurement of $\delta^{13}C_{SOC}$ and $\delta^{13}C_{root}$

After air-drying, soil samples were filtered to remove visible stones and plant residue. Subsequently, The samples were ground and sieved through a 100-mesh sieve before uniform mixing. To remove carbonates, a 2-g portion of the soil samples was reacted for

24 h with an excess 1 mol/L HCl at room temperature. Subsequently, the soil samples were washed with distilled water until pH was neutral, dried at 50 °C, and then passed through a 100-mesh sieve.

The plant samples were washed, air-dried, and oven-dried at 65 °C. Next, they were pulverized in a plant grinder and passed through a 100-mesh sieve. Approximately 2 mg of ground plant material was placed at the base of a preheated quartz tube, followed by the addition of excess CuO (2–3 g). The mixture was vacuum-purified and sealed. Combustion took place in an 850 °C muffle furnace for 2 h; then, all organic carbon was converted to CO_2. The resultant CO_2 was purified, collected in crushable glass-sealed tubes using an alcohol–liquid nitrogen trap plus a custom vacuum purification system, and analyzed in a MAT-252 mass spectrometer (Thermo Finnigan Corp., San Jose, CA, USA). The $\delta^{13}C$ values of soil organic carbon and plant material were −21.808 (0.200)‰ and −28.352 (0.292)‰, respectively.

2.5. Estimation of $\delta^{13}C$ of Soil-Respired CO_2

The carbon isotope values for soil-respired CO_2 were based mainly on the Keeling plot [43,44]. The basic principle is as follows:

$$C_1 = C_0 + C_2, \quad (3)$$

where C_1, C_0, and C_2 represent the gaseous CO_2 concentration in the static chamber, the baseline CO_2 concentration, and the additional CO_2 concentration, respectively. Multiplying each component of Equation (3) by its corresponding CO_2 isotope ratio ($\delta^{13}C$) yields the mass balance equation Formula (4) for stable carbon isotope ^{13}C:

$$\delta^{13}C_1 \times C_1 = \delta^{13}C_0 \times C_0 + \delta^{13}C_2 \times C_2, \quad (4)$$

Combining Equations (3) and (4) yields Equation (5):

$$\delta^{13}C_1 = C_0 \times (\delta^{13}C_0 - \delta^{13}C_2) \times (1/C_1) + \delta^{13}C_2, \quad (5)$$

where $\delta^{13}C_2$ represents the integrated isotope ratio of CO_2 emissions from SR_a and SR_h. Therefore, $\delta^{13}C_2$ corresponds to the intercept of $\delta^{13}C_1$ versus $(1/C_1)$ on the Y-axis. Uncertainties in the keeling plot intercepts were expressed as standard errors of the intercept.

2.6. Statistical Analysis

Figures were generated in Microsoft Office 2021 and Origin 9.0. The significance of differences in the soil water content, soil temperature, soil respiration rate, and $\delta^{13}C$ of soil-respired CO_2 under various simulated rainfall treatments was assessed using a one-way ANOVA (analysis of variance) and the least significant difference (LSD) test. All statistical analyses, including the analysis of variance (ANOVA) and significance tests, were performed in SPSS 18.0 (SPSS Inc., Chicago, IL, USA). Significance was set to $p < 0.05$.

3. Results

3.1. Soil Water Content (SWC) before and after Simulated Rainfall

Despite a general increase from the pre-rainfall levels, we did not observe significant changes in the soil water content after the three simulated rainfall events (Figure 3). The average soil water content before and after the 8 mm simulated rainfall was 38.81% and 40.66% (a 4.75% increase), respectively, whereas the pre-/post-rain values were 46.07% and 46.87% (a 1.74% increase) for the 25 mm simulated rainfall in April. Similarly, the average soil water content before and after the 25 mm rainfall in June was 38.22% and 39.03% (a 2.12% increase), respectively. Notably, the increase in the post-rainfall soil water content was modest and not linearly correlated with the rainfall volume, suggesting that soil moisture does not always proportionally increase with more rain.

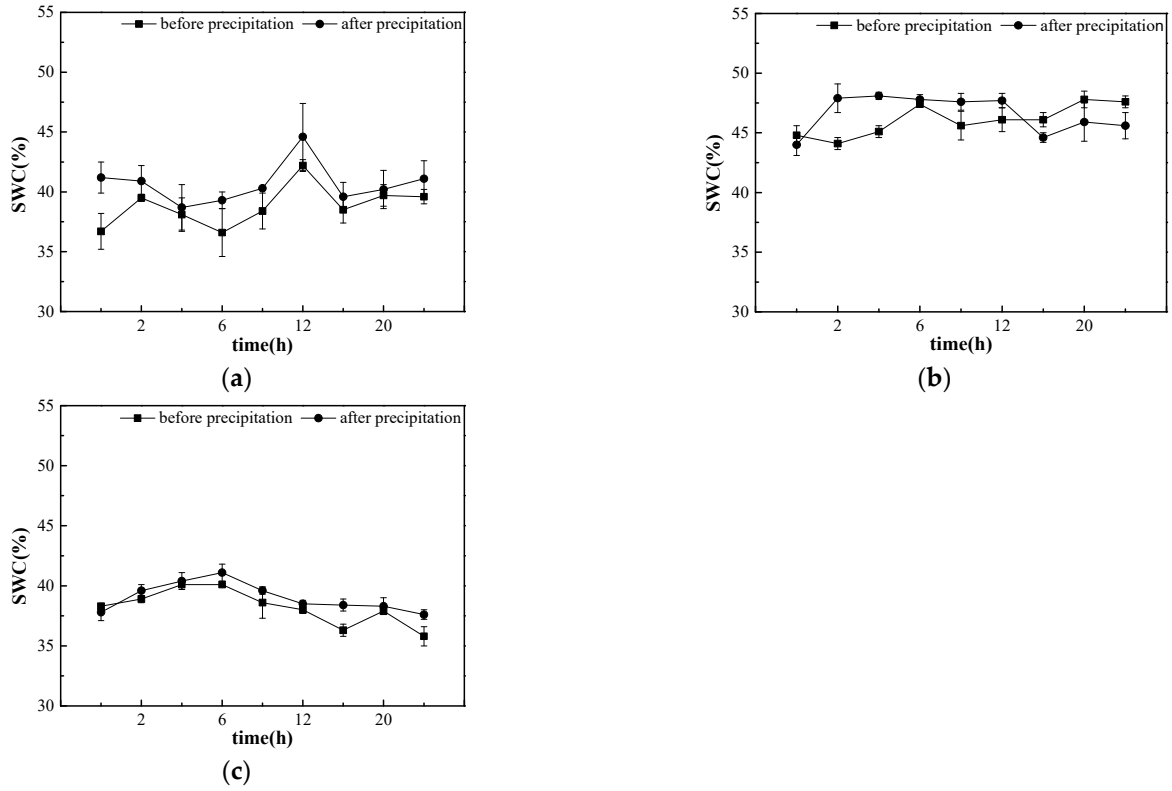


Figure 3. Changes in soil water content before and after simulated rainfall. (**a**) 8 mm simulated rainfall. (**b**) 25 mm simulated rainfall in April. (**c**) 25 mm simulated rainfall in June.

3.2. Soil Temperature before and after Simulated Rainfall

The soil temperature before 8 mm of rainfall ranged from 10.4 to 17.0 °C and then ranged from 13.8 and 17.5 °C after rainfall (Figure 4). For the 25 mm simulation in April, the soil temperature range was 15.3–16.6 °C before the rain and 17.1–17.9 °C after the rain. In contrast, the soil temperature range for the 25 mm simulation in June was 22.6–24.7 °C before the rain and 20.4–24.3 °C after the rain. The soil temperatures before and after rainfall for the 8 mm and June 25 mm simulations did not differ ($p > 0.05$, ANOVA). However, compared with that of the April-25-mm simulation, the average soil temperature before and after rainfall differed significantly, rising from 15.94 °C to 17.52 °C ($p < 0.05$, ANOVA). Notably, although the soil temperature differed significantly between pre- and post-25 mm rainfall in April, the magnitude of the difference was modest.

3.3. Changes in the Soil Respiration Rate before and after Simulated Rainfall

Overall, soil respiration rates increased following simulated rainfall to a peak and then decreased over time (Figure 5). The average soil respiration rates pre-rainfall were 183.00 $mg \cdot m^{-2} \cdot h^{-1}$ (8 mm), 375.42 $mg \cdot m^{-2} \cdot h^{-1}$ (25 mm in April), and 628.40 $mg \cdot m^{-2} \cdot h^{-1}$ (25 mm in June). Following the respective rainfall simulations, the average soil respiration rates rose to 205.31 $mg \cdot m^{-2} \cdot h^{-1}$, 558.94 $mg \cdot m^{-2} \cdot h^{-1}$, and 899.61$mg \cdot m^{-2} \cdot h^{-1}$ (or increases of 12.20%, 48.88%, and 43.16% from the pre-rainfall levels). Thus, heavy rainfall events appear to heighten CO_2 release through soil respiration.

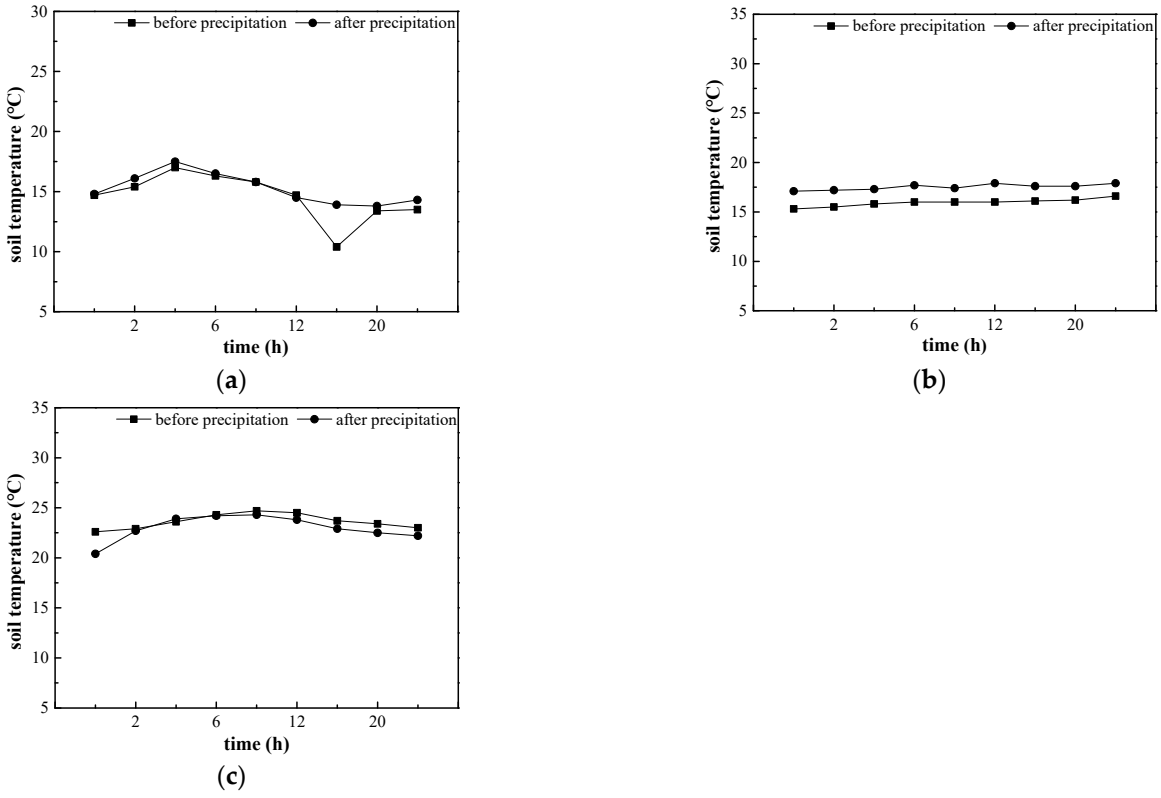


Figure 4. Changes in soil temperature before and after simulated rainfall. (**a**) 8 mm simulated rainfall. (**b**) 25 mm simulated rainfall in April. (**c**) 25 mm simulated rainfall in June.

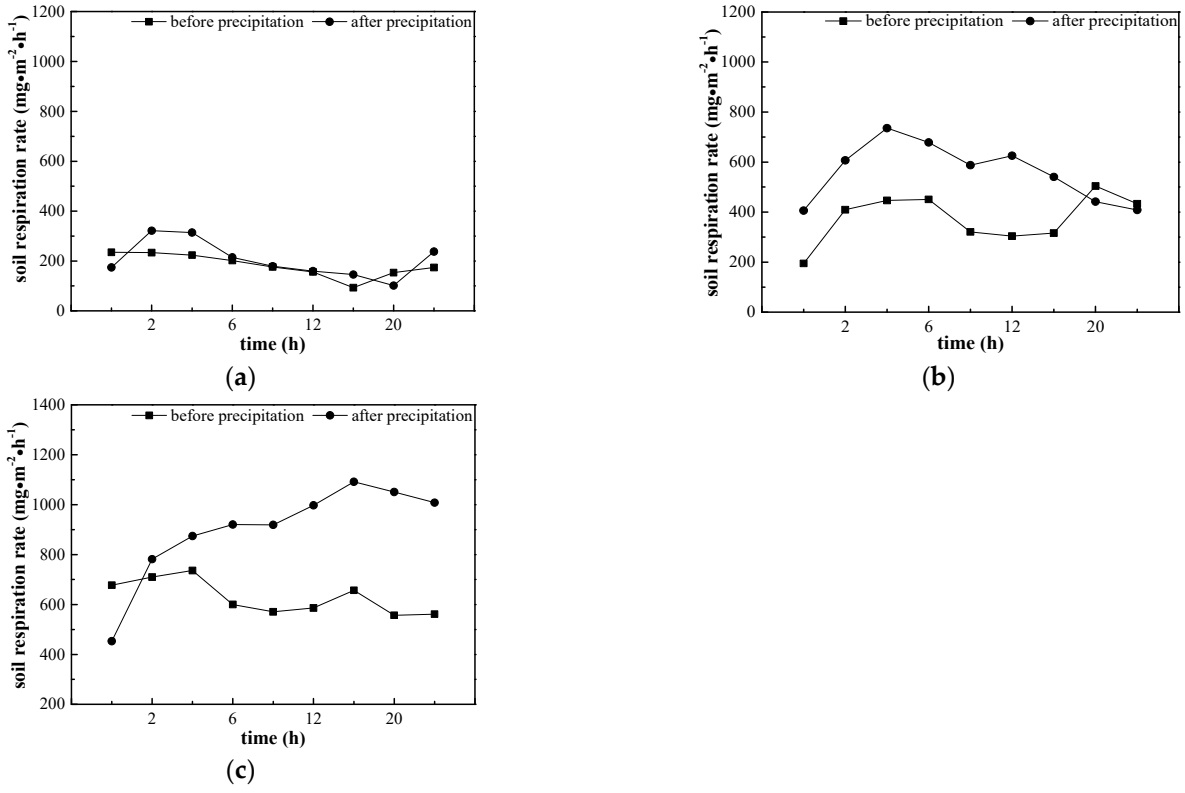


Figure 5. Soil respiration rates before and after simulated rainfall. (**a**) 8 mm simulated rainfall. (**b**) 25 mm simulated rainfall in April. (**c**) 25 mm simulated rainfall in June.

Soil respiration rates peaked at 2, 4, and 16 h after 8 mm, 25 mm (April), and 25 mm (June) of rainfall, respectively. This trend suggests that increased rainfall volume prolongs the time required to reach peak soil respiration rates. Notably, however, the latency in reaching peak soil respiration differed between the two 25-mm simulation conditions. The variance between the April and June simulations underscores the fact that soil respiration is influenced by factors beyond simply rainfall characteristics.

3.4. Changes of $\delta^{13}C$ of Soil-Respired CO_2 before and after Simulated Rainfall

Prior to the simulated rainfall, $\delta^{13}C$ ranged from −26.992‰ to −24.539‰ for 8 mm, −25.778‰ to −23.211‰ for 25 mm (April), and −25.321‰ to −23.819‰ for 25 mm (June) (Figure 6). After the simulated rainfall, the corresponding ranges were −26.119‰ to −21.601‰, −24.417‰ to −22.358‰, and −24.313‰ to −20.273‰. Significant differences in the $\delta^{13}C$ value of soil-respired CO_2 were observed before and after the simulated rainfall ($p < 0.05$, ANOVA). After the rain, the $\delta^{13}C$ of soil-respired CO_2 was enriched compared with that before the rain. The $\delta^{13}C$ of soil-respired CO_2 was initially enriched at the beginning of the rain but became depleted over time.

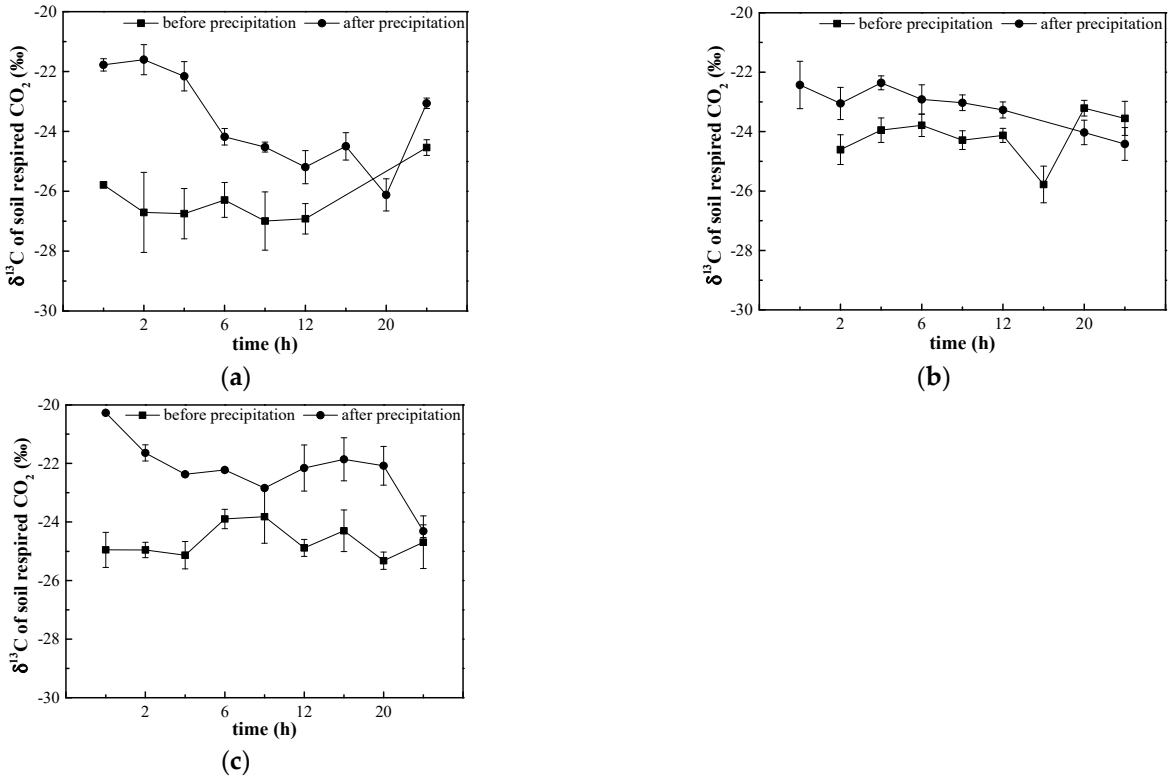


Figure 6. Variation in $\delta^{13}C$ of soil-respired CO_2 before and after simulated rainfall. (**a**) 8 mm simulated rainfall. (**b**) 25 mm simulated rainfall in April. (**c**) 25 mm simulated rainfall in June.

4. Discussion

Rainfall reportedly influences soil respiration by altering both soil temperature and moisture [45,46]. Rainfall-related changes in soil respiration are primarily driven by soil moisture fluctuations, with minimal influence from the soil temperature [5]. Similarly, our study found no significant difference in the soil temperature before and after either 8 mm or 25 mm (June) simulated rainfall (Figure 4). Notably, although the soil temperature differed significantly between pre- and post-25 mm rainfall in April, the magnitude of the difference was modest. Overall, we can conclude that, even in karst ecosystems, soil moisture is the main driver of rainfall-related changes to soil respiration, whereas the soil temperature has a minimal effect. In contrast, Tan et al. (2021) did not observe a

significant correlation between soil respiration triggered by rainfall and soil temperature in humid regions [10]. Yang et al. (2017) emphasized that the impact of precipitation on soil respiration is predominantly mediated via soil moisture levels [47]. The researchers emphasized that soil moisture played a crucial role in driving variations in soil respiration under different precipitation conditions. This relationship has a direct impact on soil respiration, and it indirectly influences soil microbial carbon pools, as well as above- and below-ground net primary productivity. Collectively, these factors explain 98% of the variability in soil respiration. The findings reported in this study are consistent with the viewpoints proposed in the existing research literature.

Importantly, post-rain fluctuations in soil moisture did not follow a clear pattern and did not directly correlate with the amount of precipitation (Figure 3). Multiple characteristics contribute to soil moisture variation after rainfall, including regional topography, soil composition, and vegetation cover [48]. These factors explain why soil moisture does not have a directly proportional relationship to the precipitation volume [49]. In this study, three simulated rainfall events were applied directly onto the soil surface, regardless of the type of vegetation present. The regulation of the flow rate prevented runoff caused by topographical factors. Therefore, the observed disproportionality was not primarily associated with the soil type. In karst regions specifically, the soil profile is shallow and highly permeable, leading to the rapid movement and depletion of water as underground runoff [50]. This feature of karst soil is likely the main reason for non-proportional fluctuations in soil moisture under varying precipitation.

Following prolonged droughts in arid regions, rainfall accelerates soil carbon mineralization, affecting microbial activity and the community structure. The result is a rapid increase in soil respiration [51–55]. However, in temperate and subtropical forests with optimal soil moisture conditions, rainfall can significantly decrease soil respiration rates [56,57]. In addition, when soil moisture is high, short periods of rainfall may saturate or even waterlog the soil. Rainfall restricts the diffusion of atmospheric O_2 into the soil, which reduces microbial activity and soil CO_2 production [58,59]. Thus, optimizing soil moisture is important for increasing soil CO_2 emissions [60]. Just as excess moisture limits respiration, sub-optimum moisture is a limiting factor in soil decomposition [61].

Our study area experiences a subtropical humid monsoon climate, but the three simulated rainfall events increased soil respiration (Figure 5), contradicting previously reported findings. In other words, the experimental water volume did not cause the soil moisture to reach a critical threshold. This phenomenon could be attributed to the distinctive ecological characteristics of the region. Karst regions are characterized by shallow soil layers, and they have a limited capacity to retain soil water. As a result, a significant amount of precipitation is lost through subsurface runoff. This leads to a decrease in the frequency of soil saturation or waterlogging. Instead, the increase in soil water content stimulated soil CO_2 emissions. A comparison of soil respiration rate changes after simulated rainfall in April and June suggests that rainfall not only alters the soil moisture content but also influences the water potential, oxygen diffusion, and dissolved matrix [62,63]. These additional effects contribute to rainfall's influence on the soil CO_2 release.

In the present study, three simulated rainfall events enhanced soil respiration. The mean values of $\delta^{13}C$ of soil-respired CO_2 before the simulated rainfall were −26.282‰, −24.163‰, and −24.661‰, whereas after the rainfall, they were −23.678‰, −23.188‰, and −22.195‰ (Figure 6). Using a two-component mixing model for calculation [64] revealed that the proportions of heterotrophic respiration to total respiration before the simulated rainfall were 33.46%, 64.98%, and 57.57%, respectively. After the rainfall, these proportions increased to 72.19%, 79.48%, and 94.24%, indicating that the post-rainfall increase in soil respiration was primarily driven by heterotrophic respiration. This finding is consistent with the results of previous studies [22,24,26].

Precipitation primarily affects SR through two mechanisms: altering the substrate supply and inducing microbial stress. Substrate changes can result from processes such as

aggregate rupture, the release of compatible solutes, microbial mortality, and the dissolution of soluble organic compounds. Aggregate rupture is the physical breakdown of soil aggregates caused by air compression and soil expansion/contraction during wet/dry cycles, respectively. This process exposes soil organic matter (previously protected via aggregates) to soil microbes, accelerating the decomposition of soil organic matter and the consequent CO_2 release [65–67].

Compatible solute release occurs under drought conditions, when soil microbes accumulate solutes in their cell membranes to prevent dehydration. Upon rehydration, cells rapidly process these solutes and release them into the soil. Other microbes then promptly assimilate and mineralize the released solutes [68–75]. Moreover, upon soil rehydration, dead microbes [68,76,77] and other soluble organic compounds [78] may serve as potential carbon substrates.

However, these data largely stem from research focusing on arid and semi-arid regions. In humid regions, increased rainfall significantly reduces dissolved organic carbon and microbial utilizable organic carbon in the soil [11]. Notably, we did not observe any instances of soil drought or semi-drought at our study site; the soil water content remained consistently above 35%. Additionally, our multiple simulated rainfall events did not appear to have lowered soil organic carbon.

The microbial stress mechanism refers to the decrease in populations and individual respiration rates among soil microbes when under drought conditions, leading to an overall decline in respiration. However, soil microbes exhibit extensive environmental adaptability, employing physiological strategies such as osmotic pressure regulation, dormancy, reactivation, and extracellular enzyme synthesis to cope with drought stress [79,80]. Thus, upon water replenishment, microbes can rapidly metabolize substrates again.

In line with this physiological flexibility, evidence shows that the wet–dry cycles triggered due to rainfall can impact microbial activity [63,81–85], abundance, species diversity [86,87], and community composition [88,89]. Evidently, such a string of influences would also alter microbial metabolic processes.

In arid and semi-arid regions, researchers have extensively utilized the manipulation of substrate availability and the application of microbial stress mechanisms to investigate the "Birch" effect. This effect is initiated via wet–dry cycles resulting from precipitation events. In this study, it is important to highlight that there were no instances of soil drought or semi-drought observed at the research site, and the soil water content consistently stayed above 35%. Hence, the mechanisms related to changes in the substrate supply and microbial stress are insufficient to fully explain the impact of rainfall on soil respiration in this specific region. Soil-dissolved organic carbon (DOC) and microbial biomass carbon (MBC) are crucial indicators of both the substrate supply alteration mechanism and the microbial stress mechanism. A meta-analysis revealed a significant decrease in soil DOC and MBC as a result of increased precipitation in the humid regions [10]. Based on the mechanisms mentioned above, despite the brief duration of the three simulated rain events in this investigation and the notable permeability of karst soils, there was only a slight decrease in soil DOC and MBC. Consequently, it was anticipated that the emission of soil CO_2 would also be reduced. However, soil respiration increased following the three simulated rain events in this study, indicating a direct correlation between the amount of precipitation and the subsequent rise in soil CO_2 emissions. There may be an alternative explanation available to clarify the soil respiration response to rainfall in this specific region.

In a moist environment, microbes typically encounter lower osmotic stress, implying increased resources and energy available for growth [90]. Transitioning from optimal moisture levels (a 50% water holding capacity) to lower levels swiftly alters microbial growth rates [91]. As we have already highlighted, post-rainfall soil respiration in this study closely aligned with the $\delta^{13}C$ values of soil organic matter, likely due to changes in soil moisture content. Thus, the experimental fluctuations in water levels probably trigger rapid changes in microbial growth rates and aid the decomposition of soil organic matter.

The main soil type at our study site was limestone. Prior research has emphasized the essential role of soil inorganic carbon as a source of CO_2 in total soil CO_2 emissions [3,92–95]. Elevating soil moisture typically causes carbonates to release more CO_2 [96–98] via two primary mechanisms. First, increased soil moisture promotes organic carbon mineralization while reducing CO_2 diffusion [99,100], raising CO_2 concentrations in the soil and inducing carbonate dissolution or precipitation [98,101]. Second, soil moisture drives the equilibrium reaction between carbonates and CO_2 [97,98,101]:

$$CaCO_{3(s)} + H_2O_{(l)} + CO_{2(g)} \leftrightarrow {Ca^{2+}}_{(aq)} + 2{HCO_3}^-{}_{(aq)} \quad (6)$$

Immediately after the simulated rainfall, we observed that $\delta^{13}C$ of CO_2 emitted from soil respiration was more enriched than $\delta^{13}C$ of soil organic matter (Figure 6). This pattern was expected because microbes tend to preferentially utilize lighter ^{12}C isotopes when decomposing organic matter, leading to a progressive enrichment of ^{13}C isotopes in the soil [102]. In other words, CO_2 produced from carbonate dissolution/precipitation is likely a contributing factor to post-rainfall elevation in CO_2 emissions from soil respiration.

5. Conclusions

In the present study, simulated rainfall enhanced soil respiration in a native karst forest, leading to CO_2 release. Isotope data indicated that the post-rainfall rise in soil CO_2 release originated mainly from heterotrophic respiration, likely stemming from changes in microbial growth conditions after rainfall increased the soil moisture. Moisture conditions also influenced carbonate dissolution and precipitation dynamics, further contributing to the post-rainfall CO_2 release. The findings of our research clarify the mechanism that governs the short-term effects of rainfall on soil respiration in karst ecosystems. The impact of precipitation on soil respiration may have long-lasting effects and exhibit variability, depending on the characteristics of the precipitation. Therefore, it is crucial to conduct extensive observations in the future to investigate the impact of rainfall on soil respiration. Furthermore, the implementation of controlled experiments is essential in accurately distinguishing the origins of soil respiration triggered by rainfall. This study aimed to investigate the interdependent relationship between soil respiration and various influencing factors, including microbial communities. The aim of this study was to establish the foundation for enhancing the carbon cycle model of karst ecosystems, thereby advancing our understanding and prediction of the cycling processes that occur within these ecosystems. This will help develop effective greenhouse gas emission reduction measures, such as water management and carbon pool management, which provide a scientific basis for addressing climate change and global warming. It is important to highlight that, when utilizing the carbon isotope natural abundance method to differentiate between the various sources of soil respiration CO_2, a crucial factor to consider is the significant variability in the $\delta^{13}C$ values of soil respiration components. Limitations may arise in domains where these distinctions are not clearly discernible.

Author Contributions: W.L.: investigation, data curation, and writing—original draft preparation. X.L.: writing—review and editing and funding acquisition. H.D.: writing—review and editing and funding acquisition. All authors have read and agreed to the published version of the manuscript.

Funding: This research was financially supported by the National Natural Science Foundation of China (40672112, 42071142) and the Guizhou Education University 2021 Annual Doctoral Project of School-level Scientific Research Fund (2021BS023).

Data Availability Statement: The data presented in this study are available upon request from the authors.

Conflicts of Interest: The authors declare no conflicts of interest.

References

1. Ahirwal, J.; Maiti, S.K.; Singh, A.K. Changes in ecosystem carbon pool and soil CO_2 flux following post-mine reclamation in dry tropical environment, India. *Sci. Total Environ.* **2017**, *583*, 153–162. [CrossRef] [PubMed]
2. Endsley, K.A.; Kimball, J.S.; Reichle, R.H. Soil respiration phenology improves modeled phase of terrestrial net ecosystem exchange in northern hemisphere. *J. Adv. Model. Earth Syst.* **2022**, *14*, e2021MS002804. [CrossRef]
3. Zamanian, K.; Zarebanadkouki, M.; Kuzyakovy, Y. Nitrogen fertilization raises CO_2 efflux from inorganic carbon: A global assessment. *Glob. Chang. Biol.* **2018**, *24*, 2810–2817. [CrossRef] [PubMed]
4. Schlesinger, W.H.; Andrews, J.A. Soil respiration and the global carbon cycle. *Biogeochemistry* **2000**, *48*, 7–20. [CrossRef]
5. Liu, L.L.; Wang, X.; Lajeunesse, M.J.; Miao, G.F.; Piao, S.L.; Wan, S.Q.; Wu, Y.X.; Wang, Z.H.; Yang, S.; Li, P.; et al. A cross-biome synthesis of soil respiration and its determinants under simulated precipitation changes. *Glob. Chang. Biol.* **2016**, *22*, 1394–1405. [CrossRef]
6. Du, Y.; Wang, Y.P.; Su, F.L.; Jiang, J.; Wang, C.; Yu, M.X.; Yan, J.H. The response of soil respiration to precipitation change is asymmetric and differs between grasslands and forests. *Glob. Chang. Biol.* **2020**, *26*, 6015–6024. [CrossRef] [PubMed]
7. Miao, Y.; Han, H.Y.; Du, Y.; Zhang, Q.; Jiang, L.; Hui, D.F.; Wan, S.Q. Nonlinear responses of soil respiration to precipitation changes in a semiarid temperate steppe. *Sci. Rep.* **2017**, *7*, 45782. [CrossRef] [PubMed]
8. Ru, J.Y.; Zhou, Y.Q.; Hui, D.F.; Zheng, M.M.; Wan, S.Q. Shifts of growing-season precipitation peaks decrease soil respiration in a semiarid grassland. *Glob. Chang. Biol.* **2018**, *24*, 1001–1011. [CrossRef] [PubMed]
9. Zhao, M.; Guo, S.L.; Wang, R. Diverse soil respiration responses to extreme precipitation patterns in arid and semiarid ecosystems. *Appl. Soil Ecol.* **2021**, *163*, 103928. [CrossRef]
10. Tan, S.Y.; Ni, X.Y.; Yue, K.; Liao, S.; Wu, F.Z. Increased precipitation differentially changed soil CO_2 efflux in arid and humid areas. *Geoderma* **2021**, *388*, 114946. [CrossRef]
11. Chen, Z.H.; Wei, X.Y.; Ni, X.Y.; Wu, F.Z.; Liao, S. Changing precipitation effect on forest soil carbon dynamics is driven by different attributes between dry and wet areas. *Geoderma* **2023**, *429*, 116279. [CrossRef]
12. Morris, K.A.; Hornum, S.; Crystal-Ornelas, R.; Pennington, S.C.; Bond-Lambery, B. Soil respiration response to simulated precipitation change depends on ecosystem type and study duration. *J. Geophys. Res. Biogeosci.* **2022**, *127*, e2022JG006887. [CrossRef]
13. Du, Y.; Wang, Y.P.; Hui, D.F.; Yan, J.H. Significant effects of precipitation frequency on soil respiration and its components-A global synthesis. *Glob. Chang. Biol.* **2023**, *29*, 1188–1205. [CrossRef] [PubMed]
14. Zhang, P.F.; Wang, D.D.; Yu, X.X.; Jia, G.D.; Liu, Z.Q.; Wang, Y.S.; Zhang, Y.E. Effects of drought and rainfall events on soil autotrophic respiration and heterotrophic respiration. *Agric. Ecosyst. Environ.* **2021**, *308*, 107267. [CrossRef]
15. Liu, W.X.; Zhang, Z.; Wan, S.Q. Predominant role of water in regulating soil and microbial respiration and their responses to climate change in a semiarid grassland. *Glob. Chang. Biol.* **2009**, *15*, 184–195. [CrossRef]
16. Talmon, Y.; Sternberg, M.; Grünzweig, J.M. Impact of rainfall manipulations and biotic controls on soil respiration in Mediterranean and desert ecosystems along an aridity gradient. *Glob. Chang. Biol.* **2011**, *17*, 1108–1118. [CrossRef]
17. Moyano, F.E.; Manzoni, S.; Chenu, C. Responses of soil heterotrophic respiration to moisture availability: An exploration of processes and models. *Soil Biol. Biochem.* **2013**, *59*, 72–85. [CrossRef]
18. Hopkins, F.; Gonzalez-meler, M.A.; Flower, C.E.; Lynch, D.J.; Czimczik, C.; Tang, J.S.; Subke, J. Ecosystem-level controls on root-rhizosphere respiration. *New Phytol.* **2013**, *199*, 339–351. [CrossRef] [PubMed]
19. Shen, W.J.; Jenerette, G.D.; Hui, D.F.; Phillips, R.P.; Ren, H. Effects of changing precipitation regimes on dryland soil respiration and C pool dynamics at rainfall event, seasonal and interannual scales. *J. Geophys. Res. Biogeosci.* **2008**, *113*, G03024. [CrossRef]
20. Sanaullah, M.; Rumpel, C.; Charrier, X.; Chabbi, A. How does drought stress influence the decomposition of plant litter with contrasting quality in a grassland ecosystem? *Plant Soil* **2012**, *352*, 277–288. [CrossRef]
21. Kopittke, G.R.; Tietema, A.; van Loon, E.E.; Asscheman, D. Fourteen annually repeated droughts suppressed autotrophic soil respiration and resulted in an ecosystem change. *Ecosystems* **2014**, *17*, 242–257. [CrossRef]
22. Zhao, C.C.; Miao, Y.; Yu, C.D.; Zhu, L.L.; Wang, F.; Jiang, L.; Hui, D.F.; Wan, S.Q. Soil microbial community composition and respiration along an experimental precipitation gradient in a semiarid steppe. *Sci. Rep.* **2016**, *6*, 24317. [CrossRef] [PubMed]
23. Moinet, G.Y.K.; Cieraad, E.; Hunt, J.E.; Fraser, A.; Turnbull, M.H.; Whitehead, D. Soil heterotrophic respiration is insensitive to changes in soil water content but related to microbial access to organic matter. *Geoderma* **2016**, *274*, 68–78. [CrossRef]
24. Zhang, B.W.; Li, S.; Chen, S.P.; Ren, T.T.; Yang, Z.Q.; Zhao, H.L.; Liang, Y.; Han, X.G. Arbuscular mycorrhizal fungi regulate soil respiration and its response to precipitation change in a semiarid steppe. *Sci. Rep.* **2016**, *6*, 19990. [CrossRef] [PubMed]
25. Huang, S.D.; Ye, G.F.; Lin, J.; Chen, K.T.; Xu, X.; Ruan, H.H.; Tan, F.L.; Chen, H.Y.H. Autotrophic and heterotrophic soil respiration responds asymmetrically to drought in a subtropical forest in the Southeast China. *Soil Biol. Biochem.* **2018**, *123*, 242–249. [CrossRef]
26. Zhang, B.W.; Li, W.J.; Chen, S.P.; Tan, X.R.; Wang, S.S.; Chen, M.L.; Ren, T.T.; Xia, J.Y.; Huang, J.H.; Han, X.G. Changing precipitation exerts greater influence on soil heterotrophic than autotrophic respiration in a semiarid steppe. *Agric. For. Meteorol.* **2019**, *271*, 413–421. [CrossRef]
27. Zhou, C.T.; Biederman, J.A.; Zhang, H.; Li, L.F.; Cui, A.Y.; Kuzyakov, Y.; Hao, Y.B. Extreme-duration drought impacts on soil CO_2 efflux are regulated by plant species composition. *Plant Soil* **2019**, *439*, 357–372. [CrossRef]

28. Bond-Lamberty, B.; Bailey, V.L.; Chen, M.; Gough, C.M.; Vargas, R. Globally rising soil heterotrophic respiration over recent decades. *Nature* **2018**, *560*, 80–83. [CrossRef] [PubMed]
29. Ehleringer, J.R.; Buchmann, N.; Flanagan, L.B. Carbon isotope ratios in belowground carbon cycle processes. *Ecol. Appl.* **2000**, *10*, 412–422. [CrossRef]
30. Hanson, P.J.; Edwards, N.T.; Garten, C.T.; Andrews, J.A. Separating root and soil microbial contributions to soil respiration: A review of methods and observations. *Biogeochemistry* **2000**, *48*, 115–146. [CrossRef]
31. Kuzyakov, Y.; Gavrichkova, O. Time lag between photosynthesis and carbon dioxide efflux from soil: A review of mechanisms and controls. *Glob. Chang. Biol.* **2010**, *16*, 3386–3406. [CrossRef]
32. Diao, H.Y.; Wang, A.Z.; Yuan, F.H.; Guan, D.X.; Wu, J.B. Autotrophic respiration modulates the carbon isotope composition of soil respiration in a mixed forest. *Sci. Total Environ.* **2022**, *807*, 150834. [CrossRef] [PubMed]
33. Lin, G.H.; Ehleringer, J.R. Carbon isotopic fractionation does not occur during dark despiration in C3 and C4 plants. *Plant Physiol.* **1997**, *114*, 391–394. [CrossRef] [PubMed]
34. Singh, J.S.; Gupta, S.R. Plant decomposition and soil respiration in terrestrial ecosystems. *Bot. Rev.* **1977**, *43*, 449–528. [CrossRef]
35. Lin, G.H.; Ehleringer, J.R.; Rygiewicz, P.T.; Johnson, M.G.; Tingey, D.T. Elevated CO_2 and temperature impacts on different components of soil CO_2 efflux in Douglas-fir terracosms. *Glob. Chang. Biol.* **1999**, *5*, 157–168. [CrossRef]
36. Bowling, D.R.; Pataki, D.E.; Randerson, J.T. Carbon isotopes in terrestrial ecosystem pools and CO_2 fluxes. *New Phytol.* **2008**, *178*, 24–40. [CrossRef]
37. Millard, P.; Midwood, A.J.; Hunt, J.E.; Barbour, M.M.; Whitehead, D. Quantifying the contribution of soil organic matter turnover to forest soil respiration, using natural abundance $\delta^{13}C$. *Soil Biol. Biochem.* **2010**, *42*, 935–943. [CrossRef]
38. Comeau, L.-P.; Lai, D.Y.F.; Cui, J.J.J.; Farmer, J. Separation of soil respiration: A site-specific comparison of partition methods. *Soil* **2018**, *4*, 141–152. [CrossRef]
39. Zhu, A.C.; Di, D.R.; Ma, M.G.; Shi, W.Y. Stable isotopes in greenhouse gases from soil: A review of theory and application. *Atmosphere* **2019**, *10*, 377. [CrossRef]
40. Ford, D.C.; Williams, P.M. *Karst Hydrogeology and Geomorphology*; John Wily and Sons Ltd.: Oxford, UK, 2007.
41. Berner, E.K.; Berner, R.A. *Global Environment: Water, Air, and Geochemical Cycles*; Princeton University Press: Princeton, NJ, USA, 2012.
42. Yan, J.H.; Wang, Y.P.; Zhou, G.Y.; Li, S.G.; Yu, G.R.; Li, K. Carbon uptake by karsts in the Houzhai Basin, Southwest China. *J. Geophys. Res. Biogeosci.* **2011**, *116*, 1–10. [CrossRef]
43. Keeling, C.D. The concentration and isotopic abundances of atmospheric carbon dioxide in rural areas. *Geochim. Cosmochim. Acta* **1958**, *13*, 322–334. [CrossRef]
44. Keeling, C.D. The concentration and isotopic abundances of carbon dioxide in rural and marine air. *Geochim. Cosmochim. Acta* **1961**, *24*, 277–298. [CrossRef]
45. Sun, Q.Q.; Meyer, W.S.; Koerber, G.R.; Marschner, P. Prior rainfall pattern determines response of net ecosystem carbon exchange to a large rainfall event in a semi-arid woodland. *Agric. Ecosyst. Environ.* **2017**, *247*, 112–119. [CrossRef]
46. Deng, Q.; Zhang, D.Q.; Han, X.; Chu, G.W.; Zhang, Q.F.; Hui, D.F. Changing rainfall frequency rather than drought rapidly alters annual soil respiration in a tropical forest. *Soil Biol. Biochem.* **2018**, *121*, 8–15. [CrossRef]
47. Yang, Q.X.; Tian, D.S.; Zeng, H.; Niu, S.L. Main factors driving changes in soil respiration under altering precipitation regimes and the controlling processes. *Chin. J. Plant Ecol.* **2017**, *41*, 1239–1250. [CrossRef]
48. Rosenbaum, U.; Bogena, H.R.; Herbst, M.; Peterson, T.J.; Weuthen, A.; Western, A.W.; Vereecken, H. Seasonal and event dynamics of spatial soil moisture patterns at the small catchment scale. *Water Resour. Res.* **2012**, *48*, W10544. [CrossRef]
49. Yu, S.Q.; Mo, Q.F.; Chen, Y.Q.; Li, Y.W.; Li, Y.X.; Zou, B.; Xia, H.P.; Jun, w.; Li, Z.A.; Wang, F.M. Effects of seasonal precipitation change on soil respiration processes in a seasonally dry tropical forest. *Ecol. Evol.* **2020**, *10*, 467–479. [CrossRef] [PubMed]
50. Yang, J.; Chen, H.S.; Nie, Y.P.; Wang, K.L. Dynamic variations in profile water on karst hillslopes in Southwest China. *Catena* **2019**, *172*, 655–663. [CrossRef]
51. McIntyre, R.E.S.; Adams, M.A.; Ford, D.J.; Grierson, P.F. Rewetting and litter addition influence mineralisation and microbial communities in soils from a semi-arid intermittent stream. *Soil Biol. Biochem.* **2009**, *41*, 92–101. [CrossRef]
52. Bowling, D.R.; Grote, E.E.; Belnap, J. Rain pulse response of soil CO_2 ecchange by biological soil crusts and grasslands of the semiarid Colorado Plateau, United States. *J. Geophys. Res. Biogeosci.* **2011**, *116*, 2415–2422. [CrossRef]
53. Yan, L.M.; Chen, S.P.; Xia, J.Y.; Luo, Y.Q. Precipitation regime shift enhanced the rain pulse effect on soil respiration in a semi-arid steppe. *PLoS ONE* **2014**, *9*, e104217. [CrossRef] [PubMed]
54. Rey, A.; Oyonarte, C.; Morán-López, T.; Raimundo, J.; Pegoraro, E. Changes in soil moisture predict soil carbon losses upon rewetting in a perennial semiarid steppe in SE Spain. *Geoderma* **2017**, *287*, 135–146. [CrossRef]
55. Zhang, Y.; Xie, Y.Z.; Ma, H.B.; Zhang, J.; Jing, L.; Wang, Y.T.; Li, J.P. The responses of soil respiration to changed precipitation and increased temperature in desert grassland in northern China. *J. Arid. Environ.* **2021**, *193*, 104579. [CrossRef]
56. Wang, Y.D.; Wang, Z.L.; Wang, H.M.; Guo, C.C.; Bao, W.K. Rainfall pulse primarily drives litterfall respiration and its contribution to soil respiration in a young exotic pine plantation in subtropical China. *Can. J. For. Res.* **2012**, *42*, 657–666. [CrossRef]
57. Liu, Y.C.; Liu, S.R.; Wang, J.X.; Zhu, X.L.; Zhang, Y.D.; Liu, X.J. Variation in soil respiration under the tree canopy in a temperate mixed forest, central China, under different soil water conditions. *Ecol. Res.* **2014**, *29*, 133–142. [CrossRef]

58. Jimenez, K.L.; Starr, G.; Staydhammer, C.L.; Schedlbauer, J.L.; Loescher, H.W.; Malone, S.L.; Oberbauer, S.F. Carbon dioxide exchange rates from short- and long-hydroperiod Everglades freshwater marsh. *J. Geophys. Res. Biogeosci.* **2012**, *117*, 12751. [CrossRef]
59. Vidon, P.; Marchese, S.; Welsh, M.; McMillan, S. Impact of precipitation intensity and riparian geomorphic characteristics on greenhouse gas emissions at the soil-atmosphere interface in a water-limited riparian zone. *Water Air Soil Pollut.* **2016**, *227*, 8. [CrossRef]
60. Luo, Y.Q.; Zhou, X. *Soil Respiration and the Environment*; Academic Press: Burlington, MA, USA, 2006.
61. Zhang, Y.; Sha, L.Q.; Wu, C.S.; Tan, Z.H.; Song, Q.H.; Liu, Y.T.; Dong, L.Y. Effects of continuous drought stress on soil respiration in a tropical rainforest in southwest China. *Plant Soil* **2015**, *394*, 343–353. [CrossRef]
62. Berdugo, M.; Delgado-Baquerizo, M.; Soliveres, S.; Hernández-Clemente, R.; Zhao, Y.C.; Gaitán, J.J.; Gross, N.; Saiz, H.; Maire, V.; Lehmann, A.; et al. Global ecosystem thresholds driven by aridity. *Science* **2020**, *367*, 787–790. [CrossRef]
63. Ni, X.Y.; Liao, S.; Wu, F.Z.; Groffman, P.M. Microbial biomass in forest soils under altered moisture conditions: A review. *Soil Sci. Soc. Am. J.* **2022**, *86*, 358–368. [CrossRef]
64. Zhang, Q.; Wu, J.J.; Lei, Y.; Yang, F.; Zhang, D.D.; Zhang, K.R.; Zhang, Q.F.; Cheng, X.L. Agricultural land use change impacts soil CO_2 emission and its ^{13}C-isotopic signature in central China. *Soil Till. Res.* **2018**, *177*, 105–112. [CrossRef]
65. Denef, K.; Zotarelli, L.; Boddey, R.M.; Six, J. Microaggregate-associated carbon as a diagnostic fraction for management-induced change in soil organic carbon in two Oxisols. *Soil Biol. Biochem.* **2007**, *39*, 1165–1172. [CrossRef]
66. Borken, W.; Matzner, E. Reappraisal of drying and wetting effects on C and N mineralization and fluxes in soils. *Glob. Chang. Biol.* **2009**, *15*, 808–824. [CrossRef]
67. Navarro-García, F.; Casermeiro, M.; Schimel, J.P. When structure means conservation: Effect of aggregate structure in controlling microbial responses to rewetting events. *Soil Biol. Biochem.* **2012**, *44*, 1–8. [CrossRef]
68. Kieft, T.L.; Soroker, E.; Firestone, M.K. Microbial biomass response to a rapid increase in water potential when dry soil is wetted. *Soil Biol. Biochem.* **1987**, *19*, 119–126. [CrossRef]
69. Kempf, B.; Bremer, E. Uptake and synthesis of compatible solutes as microbial stress responses to highosmolality environments. *Arch. Microbiol.* **1998**, *170*, 319–330. [CrossRef] [PubMed]
70. Halverson, L.J.; Jones, T.M.; Firestone, M.K. Release of intracellular solutes by four Soil bacteria exposed to dilution stress. *Soil Sci. Soc. Am. J.* **2000**, *64*, 1630–1637. [CrossRef]
71. Welsh, D.T. Ecological signifiance of compatible solute accumulation by micro-organisms: From single cells to global climate. *FEMS Microbiol. Rev.* **2000**, *24*, 263–290. [CrossRef] [PubMed]
72. Warren, C.R. Isotope pool dilution reveals rapid turnover of small quaternary ammonium compounds. *Soil Biol. Biochem.* **2019**, *131*, 90–99. [CrossRef]
73. Chowdhury, T.R.; Lee, J.Y.; Bottos, E.M.; Brislawn, C.J.; White III, R.A.; Bramer, L.M.; Brown, J.; Zucker, J.D.; Kim, Y.-M.; Jumpponen, A.; et al. Metaphenomic responses of a native prairie soil microbiome to moisture perturbations. *Msystems* **2019**, *4*, 1128. [CrossRef]
74. Malik, A.A.; Swenson, T.; Weihe, C.; Morrison, E.; Martiny, J.B.H.; Brodie, E.L.; Northen, T.R.; Allison, S.D. Physiological adaptations of leaf litter microbial communities to long-term drought. *Cold Spring Harb. Lab.* **2019**, *8*, 631077. [CrossRef]
75. Slessarev, E.W.; Lin, Y.; Jiménez, B.Y.; Homyak, P.M.; Chadwick, O.A.; D'Antonio, C.M.; Schimel, J.P. Cellular and extracellular C contributions to respiration after wetting dry soil. *Biogeochemistry* **2020**, *147*, 307–324. [CrossRef]
76. Blazewicz, S.J.; Schwartz, E.; Firestone, M.K. Growth and death of bacteria and fungi underlie rainfall-induced carbon dioxide pulses from seasonally dried soil. *Ecology* **2014**, *95*, 1162–1172. [CrossRef] [PubMed]
77. Blazewicz, S.J.; Hungate, B.A.; Koch, B.J.; Nuccio, E.E.; Morrissey, E.; Brodie, E.L.; Schwartz, E.; Pett-Ridge, J.; Firestone, M.K. Taxon-specific microbial growth and mortality patterns reveal distinct temporal population responses to rewetting in a California grassland soil. *ISME J.* **2020**, *14*, 1520–1532. [CrossRef] [PubMed]
78. Blankinship, J.C.; Schimel, J.P. Biotic versus abiotic controls on bioavailable soil organic carbon. *Soil Syst.* **2018**, *2*, 10. [CrossRef]
79. Barnard, R.L.; Osborne, C.A.; Firestone, M.K. Responses of soil bacterial and fungal communities to extreme desiccation and rewetting. *ISME J.* **2013**, *7*, 2229–2241. [CrossRef] [PubMed]
80. Brangarí, A.C.; Lyonnard, B.; Rousk, J. Soil depth and tillage can characterize the soil microbial responses to drying-rewetting. *Soil Biol. Biochem.* **2022**, *173*, 108806. [CrossRef]
81. Doughty, C.E.; Metcalfe, D.B.; Girardin, C.A.J.; Amézquita, F.F.; Cabrera, D.G.; Huasco, W.H.; Silva-Espejo, J.E.; Araujo-Murakami, A.; da Costa, M.C.; Feldpausch, T.R.; et al. Drought impact on forest carbon dynamics and fluxes in Amazonia. *Nature* **2015**, *519*, 79–82. [CrossRef]
82. Hinko-Najera, N.; Fest, B.; Livesley, S.J.; Arndt, S.K. Reduced throughfall decreases autotrophic respiration, but not heterotrophic respiration in a dry temperate broadleaved evergreen forest. *Agric. For. Meteorol.* **2015**, *200*, 66–77. [CrossRef]
83. Ren, C.J.; Zhao, F.Z.; Shi, Z.; Chen, J.; Han, X.H.; Yang, G.H.; Feng, Y.Z.; Ren, G.X. Differential responses of soil microbial biomass and carbon-degrading enzyme activities to altered precipitation. *Soil Biol. Biochem.* **2017**, *115*, 1–10. [CrossRef]
84. Xiao, W.; Chen, X.; Jing, X.; Zhu, B. A meta-analysis of soil extracellular enzyme activities in response to global change. *Soil Biol. Biochem.* **2018**, *123*, 21–32. [CrossRef]
85. Akinyemi, D.S.; Zhu, Y.K.; Zhao, M.Y.; Zhang, P.J.; Shen, H.H.; Fang, J.Y. Response of soil extracellular enzyme activity to experimental precipitation in a shrub-encroached grassland in Inner Mongolia. *Glob. Ecol. Conserv.* **2020**, *23*, e01175. [CrossRef]

86. Shi, A.D.; Marschner, P. Soil respiration and microbial biomass in multiple drying and rewetting cycles: Effect of glucose addition. *Geoderma* **2017**, *305*, 219–227. [CrossRef]
87. Wang, X.; Zhang, Q.; Zhang, Z.J.; Li, W.J.; Liu, W.C.; Xiao, N.J.; Liu, H.Y.; Wang, L.Y.; Li, Z.X.; Ma, J.; et al. Decreased soil multifunctionality is associated with altered microbial network properties under precipitation reduction in a semiarid grassland. *IMeta* **2023**, *2*, e106. [CrossRef]
88. Bahram, M.; Hildebrand, F.; Forslund, S.K.; Anderson, J.L.; Soudzilovskaia, N.A.; Bodegom, P.M.; Bengtsson-Palme, J.; Anslan, S.; Coelho, L.P.; Harend, H.; et al. Structure and function of the global topsoil microbiome. *Nature* **2018**, *560*, 233–237. [CrossRef] [PubMed]
89. Preece, C.; Verbruggen, E.; Liu, L.; Weedon, J.T.; Peñuelas, J. Effects of past and current drought on the composition and diversity of soil microbial communties. *Soil Biol. Biochem.* **2019**, *131*, 28–39. [CrossRef]
90. Brangarí, A.C.; Manzoni, S.; Rousk, J. A soil microbial model to analyze decoupled microbial growth and respiration during soil drying and rewetting. *Soil Biol. Biochem.* **2000**, *148*, 107871. [CrossRef]
91. Cruz-Paredes, C.; Tájmel, D.; Rousk, J. Can moisture affect temperature dependences of microbial growth and respiration? *Soil Biol. Biochem.* **2021**, *156*, 108223. [CrossRef]
92. Raza, S.; Miao, N.; WANG, P.Z.; Ju, X.T.; Chen, Z.J.; Zhou, J.B.; Kuzyakoc, Y. Dramatic loss of inorganic carbon by nitrogen-induced soil acidification in Chinese Croplands. *Glob. Chang. Biol.* **2020**, *26*, 3738–3751. [CrossRef]
93. Zamanian, K.; Zhou, J.B.; Kuzyakovy, Y. Soil carbonates: The unaccountted, irrecoverable carbon source. *Geoderma* **2021**, *384*, 114817. [CrossRef]
94. Song, X.-D.; Yang, F.; Wu, H.-Y.; Zhang, J.; Li, D.-C.; Liu, F.; Zhao, Y.-G.; Yang, J.-L.; Ju, B.; Cai, Z.-F.; et al. Significant loss of soil inorganic carbon at the continental scale. *NSR* **2022**, *9*, nwab120. [CrossRef] [PubMed]
95. Sun, Z.A.; Meng, F.Q.; Zhu, B. Influencing factors and partitioning methods of carbonate contribution to CO_2 emissions from calcareous soils. *Soil Ecol. Lett.* **2023**, *5*, 6–20. [CrossRef]
96. Stevenson, B.A.; Verburg, P.S.J. Effluxed CO_2-^{13}C from sterilized and unsterilized treatments of a calcareous soil. *Soil Biol. Biochem.* **2006**, *38*, 1727–1733. [CrossRef]
97. Dong, Y.J.; Cai, M.; Zhou, J.B. Effects of moisture and carbonate additions on CO_2 emission from calcareous soil during closed-jar incubation. *J. Arid. Land.* **2014**, *6*, 37–43. [CrossRef]
98. Lardner, T.; George, S.; Tibbett, M. Interacting controls on innate sources of CO_2 efflux from a calcareous arid zone soil under experimental acidification and wetting. *J. Arid. Environ.* **2015**, *122*, 117–123. [CrossRef]
99. Nobel, P.S.; Palta, J.A. Soil O_2 and CO_2 effects on root respiration of cacti. *Plant Soil* **1989**, *120*, 263–271. [CrossRef]
100. Serrano-Ortiz, P.; Roland, M.; Sanchez-Moral, S.; Janssens, I.A.; Domingo, F.; Goddérs, Y.; Kowalski, A.S. Hidden, abiotic CO_2 flows and gaseous reservoirs in the terrestrial carbon cycle: Review and perspectives. *Agric. For. Meteorol.* **2010**, *150*, 321–329. [CrossRef]
101. Inglima, I.; Alberti, G.; Bertolini, T.; Vaccari, F.P.; Gioli, B.; Miglietta, F.; Cotrufo, M.F.; Peressotti, A. Precipitation pulses enhance respiration of Mediterranean ecosystems: The balance between organic and inorganic components of increased soil CO_2 efflux. *Glob. Chang. Biol.* **2009**, *15*, 1289–1301. [CrossRef]
102. Diochon, A.; Kellman, L. Natural abundance measurements of ^{13}C indicate increased deep soil carbon mineralization after forest disturbance. *Geophys. Res. Lett.* **2008**, *35*, L14402. [CrossRef]

Disclaimer/Publisher's Note: The statements, opinions and data contained in all publications are solely those of the individual author(s) and contributor(s) and not of MDPI and/or the editor(s). MDPI and/or the editor(s) disclaim responsibility for any injury to people or property resulting from any ideas, methods, instructions or products referred to in the content.